Bioactive Materials 25 (2023) 95–106

Contents lists available at ScienceDirect

Bioactive Materials

journal homepage: www.keaipublishing.com/en/journals/bioactive-materials

Gold nanoparticles-embedded ceria with enhanced antioxidant activities for treating inflammatory bowel disease

Mingyi Li [a,b,d,1], Jia Liu [a,d,1], Lin Shi [a,b,d], Cheng Zhou [a,c,d], Meizhen Zou [a,b,d], Daan Fu [a,c], Ye Yuan [a,c], Chundong Yao [a,d], Lifang Zhang [b], Sumei Qin [a,d], Miaodeng Liu [a,b,d], Qian Cheng [a,b,d], Zheng Wang [a,c,d,*], Lin Wang [a,b,d,**]

[a] Research Center for Tissue Engineering and Regenerative Medicine, Union Hospital, Tongji Medical College, Huazhong University of Science and Technology, Wuhan, 430022, China
[b] Department of Clinical Laboratory, Union Hospital, Tongji Medical College, Huazhong University of Science and Technology, Wuhan, 430022, China
[c] Department of Gastrointestinal Surgery, Union Hospital, Tongji Medical College, Huazhong University of Science & Technology, Wuhan, 430022, China
[d] Hubei Key Laboratory of Regenerative Medicine and Multi-disciplinary Translational Research, Wuhan, 430022, China

ARTICLE INFO

Keywords:
Nanozyme
Inflammatory bowel disease
Reactive oxygen species
Ceria nanoparticles
Antioxidant

ABSTRACT

The excessive reactive oxygen species (ROS) is a hallmark associated with the initiation and progression of inflammatory bowel disease (IBD), which execrably form a vicious cycle of ROS and inflammation to continually promote disease progression. Here, the gold nanoparticles-embedded ceria nanoparticles (Au/CeO_2) with enhanced antioxidant activities are designed to block this cycle reaction for treating IBD by scavenging overproduced ROS. The Au/CeO_2 with core-shell and porous structure exhibits significantly higher enzymatic catalytic activities compared with commercial ceria nanoparticles, likely due to the effective exposure of catalytic sites, higher content of Ce (III) and oxygen vacancy, and accelerated reduction from Ce (IV) to Ce (III). Being coated with negatively-charged hyaluronic acid, the Au/CeO_2@HA facilitates accumulation in inflamed colon tissues via oral administration, reduces pro-inflammatory cytokines, and effectively alleviates colon injury in colitis mice. Overall, the Au/CeO_2@HA with good biocompatibility is a promising nano-therapeutic for treating IBD.

1. Introduction

Inflammatory bowel disease (IBD) is a chronic inflammatory syndrome of intestine, mainly including ulcerative colitis (UC) and Crohn's disease (CD). Such inflammatory diseases are incurable and severely impair patients' quality of life by diarrhea, abdominal pain, bloody stools, and other extraintestinal manifestations (e.g., arthritis, psoriasis, and spondylitis) [1,2]. The mainstay treatment agents for IBD include aminosalicylates, corticosteroids, antibiotics, and immunomodulatory agents aiming to alleviate inflammation and maintain remission. However, these medications are limitedly effective and associated with serious side effects [3], resulting in low patient compliance and economic burden. Biological agents (e.g., infliximab, adalimumab, natalizumab) offer an alternative opportunity for patients that show inadequate responses to standard medicine, but they suffer from limited clinical remission rate, long-term safety, and immunogenicity [4–6]. Therefore, it is highly desirable to develop innovative strategies for IBD treatment.

Despite the etiology of IBD remains unclear, extensive evidence reveals that elevated reactive oxygen species (ROS) is a hallmark in the initiation [7,8] and during progression [9–11] of IBD, which correlates with clinical features and IBD-associated colorectal cancer [12]. During the inflammatory episodes, the intestinal mucosa is infiltrated with inflammatory cells [10], and these activated immune cells continuously

Peer review under responsibility of KeAi Communications Co., Ltd.
* Corresponding author. Research Center for Tissue Engineering and Regenerative Medicine, Union Hospital, Tongji Medical College, Huazhong University of Science and Technology, Wuhan, 430022, China.
** Corresponding author. Research Center for Tissue Engineering and Regenerative Medicine, Union Hospital, Tongji Medical College, Huazhong University of Science and Technology, Wuhan, 430022, China.
E-mail addresses: zhengwang@hust.edu.cn (Z. Wang), lin_wang@hust.edu.cn (L. Wang).
[1] The authors contributed equally to this work.

https://doi.org/10.1016/j.bioactmat.2023.01.015
Received 3 November 2022; Received in revised form 16 January 2023; Accepted 16 January 2023

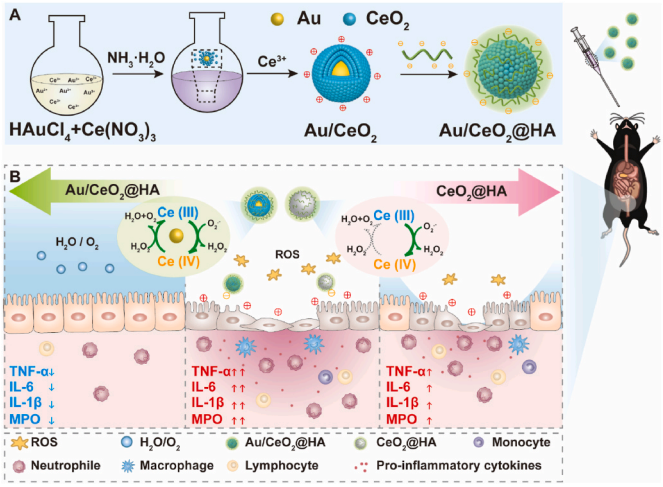

Scheme 1. Schematic illustration of the synthesis and therapy application of Au/CeO_2@HA nanozyme for mice with colitis. (A) Schematic illustration of synthesis progress of Au/CeO_2@HA. (B) Therapeutic effects of Au/CeO_2@HA or CeO_2@HA in colitis. The enhanced catalytic activity of Au/CeO_2@HA is attributed to the porous structure and accelerated the regeneration of Ce (III) from Ce (IV) induced by the Au core. The Au/CeO_2@HA sufficiently eliminates ROS and reduces pro-inflammatory cytokines to alleviate colon injury in colitis mice.

produce and release free radicals [12], resulting in oxidative stress. The excessive ROS crushes innate antioxidant systems and oxidizes biomolecules (proteins, lipids, and nucleic acids) [13] to cause intestinal epithelium damage. The chain reactions further increase the infiltration of inflammatory cells and promote the production of ROS and inflammatory cytokines. The vicious cycle of ROS and inflammation continually advances the progression of IBD [14,15]. Hence, re-establishing redox homeostasis to block this cycle reaction would be a promising strategy for treating IBD.

Exogenous natural antioxidant enzymes have been used to neutralize ROS or suppress inflammation for IBD treatment [16–20], which however are limited by low stability, high cost, and potential immunogenicity. With the development of nanotechnology, nanomaterials with enzymatic catalytic activities (named nanozymes [21]) have attracted extensive attention as potential candidates for modulating redox homeostasis in IBD [22–28]. As a representative nanozyme, ceria nanoparticles have been found to possess unique superoxide dismutase (SOD) and catalase (CAT)-mimic activities, which are widely harnessed in the treatment of ROS-related diseases such as androgenetic alopecia [29], hepatic injury [30,31], kidney injury [32], Alzheimer's disease [33,34] and stroke [35], and demonstrated to be biocompatible *in vitro* and *in vivo* [36]. The SOD- and CAT-mimetic activities of ceria originate from the co-existence of cerium (III) and cerium (IV) on the surface. The cerium (III) mainly takes advantage of SOD-mimetic activity to remove $O_2^{\bullet-}$ associated with oxidization of cerium (III) to cerium (IV), whereas the cerium (IV) decomposes H_2O_2 to mimic CAT associated with reduction of cerium (IV) [37,38]. Thus, ceria's catalytic activities are highly dependent on the regenerative redox switching between cerium (III) and cerium (IV) [38,39]. However, the reduction rate from cerium (IV) to cerium (III) is impeded because this process is energetically unfavorable [40,41]. Accelerating the regeneration from cerium (IV) to cerium (III) by facilitating electron transfer might be a feasible strategy to optimize the enzymatic activity of ceria, which would facilitate a safe and economical implementation for IBD treatment.

Herein, we synthesized gold nanoparticles-embedded ceria nanoparticles (Au/CeO_2) with enhanced SOD- and CAT-mimetic activities for treating IBD (Scheme 1). The Au/CeO_2 with core-shell and porous structure could offer a high surface-to-volume for exposure of catalytic sites, and promote cerium (III)/cerium (IV) redox reaction to enhance the antioxidant enzymatic activity of ceria. After being coated with negatively-charged hyaluronic acid (HA), the Au/CeO_2@HA facilitated accumulation in the inflamed colon tissues via oral administration, reduced the production of pro-inflammatory cytokines, and effectively alleviated colon injury in the acute colitis mice. Notably, Au/CeO_2@HA exhibited good compatibility *in vitro* and *in vivo*, which showed negligible cytotoxicity and hemolytic activity and hardly affected the major organs. These together indicate that Au/CeO_2@HA is a promising nanoantioxidant for treating IBD.

2. Materials and methods

2.1. Materials

Cerium nitrate hexahydrate and ammonia solution (AR, 25–28%) were purchased from Sinopharm chemical regent Co., Ltd (Shanghai, China). Gold chloride hydrate, cerium oxide (20–50 nm), dextran sulfate sodium (DSS), and rhodamine B were purchased from Aladdin Industrial Corporation (Shanghai, China). Methylthiazolyldiphenyl-tetrazolium bromide (MTT) was obtained from Biosharp. 2′,7′-Dichlorofluorescin diacetate (DCFH-DA) was purchased from Beyotime Chemical Reagent (Jiangsu, China). Lysotracker was purchased from Yeasen Biotech Co., Ltd (Shanghai, China). The dopamine-grafted hyaluronic acid (40–100 kDa, modification degree: 37.6 μmol/g) was synthesized as our previous work [42]. The ceria nanoparticles were synthesized as the previous studies (CeO_2-1 [27] and CeO_2-2 [43]).

2.2. Synthesis of Au/CeO_2 and Au/CeO_2@HA

Au/CeO_2 was synthesized according to the literature [44]. $HAuCl_4$ (0.024 M, 600 μL) and $Ce(NO_3)_3$ (0.1 M, 1400 μL) were added to H_2O (50 mL) in an ice bath. Next, ammonia solution (64 μL of 25–28% ammonia solution dissolved in 3 mL of H_2O) was rapidly added and stirred for 25 s. Then $Ce(NO_3)_3$ solution (0.0467 M, 3000 μL) was added to the mixed solution and stirred for 15 min. The products were collected by centrifugation (10 °C, 10000 g, and 60 min) and washing with H_2O for three times.

To modify Au/CeO_2 with hyaluronic acid (HA) shell, the Au/CeO_2 (1 mg/mL, 20 mL) was slowly added into the dopamine grafted-HA solution (1 mg/mL, 20 mL) and then stirred for 12 h. Au/CeO_2@HA was collected by centrifuging (10 °C, 10000 g, and 60 min) and washing with H_2O for three times.

To obtain the rhodamine B labeled nanoparticles, Au/CeO_2 suspension (1 mg/mL, 20 mL) was mixed with rhodamine B (1 mg/mL, 20 mL) and incubated for 4 h at room temperature. The rhodamine B-labeled Au/CeO_2 was collected by centrifuging (10000 g, and 60 min) and washing with deionized water until the supernatant is transparent. To obtain rhodamine B-labeled Au/CeO_2@HA, rhodamine B- labeled Au/CeO_2 (1 mg/mL, 10 mL) was added into the dopamine-grafted HA solution (1 mg/mL, 10 mL) and then stirred for 12 h. The rhodamine B-labeled Au/CeO_2@HA was collected by centrifuging and washing.

2.3. Characterization

Hydrodynamic size and zeta potential were measured in the deionized water on Nano-ZS ZEN3600 (Malvern). The morphology of nanoparticles was characterized by the transmission electron microscope (Hitachi H-7000FA) and high-resolution transition electron microscope (HR-TEM) (Jeol2100f). Jed2300 was used to observe the element distribution of Au/CeO_2. X-ray powder diffraction (XRD) patterns were recorded by Bruker D8 Advance. X-ray photoelectron spectroscopy (XPS) spectra were performed by ESCALAB 250Xi (Thermo Fisher). Thermogravimetric analysis (TGA) was carried out by TA TGA55. Temperature-programmed reduction (TPR) analysis was measured by AutoChem1 II 2920. The N_2 adsorption/desorption isotherm was performed by ASAP 2460 3.01 (Micromeritics, USA), and the surface area

and pore size were calculated using the Brunauer-Emmett-Teller (BET) model. Inductively coupled plasma mass spectrometry (ICP-MS, ThermoFisher iCAP-TQ) was employed to measure the retained concentrations of Au/CeO_2 or Au/CeO_2@HA in the colon tissues.

The cellular internalization of rhodamine B-labeled nanoparticles was evaluated using a Nikon Ti–U microscopy equipped with a CSU-X1 spinning-disk confocal unit (Yokogawa) and an EM-CCD camera (iXon+; Andor).

2.4. The enzymatic catalytic activity

The antioxidant activities of Au/CeO_2, CeO_2, Au/CeO_2@HA, and CeO_2@HA were conducted according to the protocols of assays kit. The $O_2^{\bullet-}$ scavenging activity was measured using a total superoxide dismutase (SOD) colorimetric assay kit (Elabscience, China). The H_2O_2 scavenging activity was measured using a catalase assay kit (Beyotime Biotechnology, China). The steady-state kinetic assay of Au/CeO_2 was determined by varying the concentration of H_2O_2 (0–15 mM) in the presence of Au/CeO_2 (50 μg/mL). After incubation at room temperature for 10 min, the residual H_2O_2 was quantified using a hydrogen peroxide assay kit (Beyotime Biotechnology, China). The K_m was calculated using Lineweaver-Burk plots [45]. To investigate the stability of Au/CeO_2@HA, Au/CeO_2@HA was dispersed and incubated in simulated gastric fluid (SGF) for 4 h or simulated intestinal fluid (SIF) for 72 h, and the hydrodynamic size, zeta potential, and enzymatic catalytic activity were measured.

2.5. Cell culture and cytotoxicity assay

Human immortalized colonic epithelial cells (NCM460) were cultured in the high glucose-DMEM media (Gibco, USA) containing 10% fetal bovine serum (FBS, ScienCell, USA) under an atmosphere of 5% CO_2 at 37 °C. NCM460 cells were cultured in 96-well plates (6×10^3 cells per well) for 24 h. After that, Au/CeO_2 or Au/CeO_2@HA (25–400 μg/mL) was added and cultured with cells for another 24 h. MTT assay was employed to quantify the cell viability.

2.6. Intracellular ROS scavenging ability

NCM460 cells were seeded at 2×10^5 cells per well in 6-well plates. After culture for 24 h, fresh media with nanoparticles (100 μg/mL) were added and cultured with cells for 12 h. Then 50 μg/mL of Rosup was added to the cells followed by incubation for 30 min. Next, the NCM460 cells were incubated with 10 μM of 2′,7′-dichlorofluorescin diacetate (DCFH-DA) for 30 min, and then washed with PBS. At last, intracellular DCF fluorescence was imaged using a fluorescence spectrophotometer (Olympus IX73 microscope). The untreated cells served as the control.

2.7. Cellular internalization behavior

HUVEC cells (human umbilical vein endothelial cells) or NCM460 cells (immortalized human colon mucosal epithelial cells) were seeded onto the cover-glass bottom dishes with a density of 6×10^4 cells and cultured for 24 h. Then the cells were incubated with rhodamine B-labeled Au/CeO_2 or Au/CeO_2@HA (100 μg/mL) for 4 h. Next, the cells were washed with PBS and stained with lysotracker Green (75 nM) and Hoechst (5 μg/mL). Finally, the cells were rinsed with PBS and imaged by a confocal fluorescence microscope.

2.8. Cytoprotective effect of nanozyme

NCM460 cells (6×10^3 cells per well) were cultured in 96-well plates for 24 h. Then, the fresh media with different concentrations of nanozymes (0, 50, 75, 100, 200 μg/mL) and H_2O_2 (300 μM) were added to the cells and incubated for another 24 h. MTT assay was employed to determine the cell viability.

2.9. Hemolysis assay

The hemolysis experiments were measured as the previous study [46]. The nanoparticles (100 μL, in PBS) were mixed with mouse red blood cell suspension (2% in PBS, v/v, 900 μL). The final concentrations of Au/CeO_2 or Au/CeO_2@HA in RBCs suspensions were 6.25–200 μg/mL. Then, the mixtures were shaken at 37 °C for 4 h and then centrifuged at 3000 rpm for 10 min. To determine the hemoglobin concentration of the supernatant, a microplate reader was used to measure the absorbance at 545 nm. Triton X-100 and PBS were chosen as the positive and negative controls.

2.10. Animal studies

Six-week-old male C57BL/6 mice were purchased from SPF (Beijing) Biotechnology Co., Ltd. All the animal experiments were performed following the guideline approved by the Institution Animal Care and Use Committee (IACUC) at Tongji Medical College, Huazhong University of Science and Technology, Wuhan, China.

2.11. Biocompatibility of Au/CeO_2@HA in vivo

The C57BL/6 mice (6-week-old, 18–20 g) acclimatized for five days and were randomly divided into two groups, including the healthy control group and Au/CeO_2@HA group ($n = 5$). Control healthy mice were given water only, and Au/CeO_2@HA group mice received 2 mg/kg of Au/CeO_2 via oral administration on day 2, 4, and 6, respectively. Changes in body weight were monitored daily. All mice were sacrificed on day 10. The colon, heart, liver, spleen, lung, and kidney were collected and fixed with 4% paraformaldehyde for hematoxylin and eosin (H&E) staining. The serum was collected for biochemical index detection.

2.12. Colon accumulation and excretion of Au/CeO_2@HA

The C57BL/6 mice (6-week-old, 18–20 g) were fed with DSS (40 kDa)-containing water (3%, w/v) for six consecutive days to establish the colitis model [47]. Next, the mice were randomly divided into two groups and were orally administered with Au/CeO_2 or Au/CeO_2@HA (2 mg/kg). After different time points (6, 12, 24, 72, 168 h), mice were sacrificed and the whole colons were collected. The colons were gently washed with PBS to remove retained feces. Next, the colon tissues were cut up into pieces and digested with aqua regia under 120 °C. After evaporation, the residues were dissolved in nitric acid (5%), and the Ce contents were determined by ICP-MS. The relative Ce accumulation was calculated by the following equation: Ce content (%) $= M_t/M_0$, where M_t is the Ce mass in colons at the indicated time, and M_0 is the total Ce mass of administered Au/CeO_2@HA or Au/CeO_2.

To visualize the distribution of Au/CeO_2@HA, the colitis mice were orally administered with rhodamine B-labeled Au/CeO_2@HA (2 mg/kg), the GI tracts were isolated, and the fluorescent images of GI tracts were obtained by *in vivo* imaging system (IVIS, Bruker, Ex = 550 nm; Em = 600 nm).

2.13. DSS-induced model of colitis

The C57BL/6 mice (6-week-old, 18–20 g) were acclimatized for five days and randomly divided into four groups, including the healthy control group, DSS-induced colitis group, DSS-induced colitis mice treated with Au/CeO_2@HA, and DSS-induced colitis group treated with CeO_2@HA ($n = 7$). Colitis mice were induced by feeding with DSS-containing water (3%) for 6 days, while the healthy mice were only fed with water. Then the colitis mice were orally treated with Au/CeO_2@HA or CeO_2@HA (2 mg/kg) on predetermined days (day 7, day 9, and day 11). The body weights of mice were recorded daily over the experimental period. On day 12, the entire colons and serum were

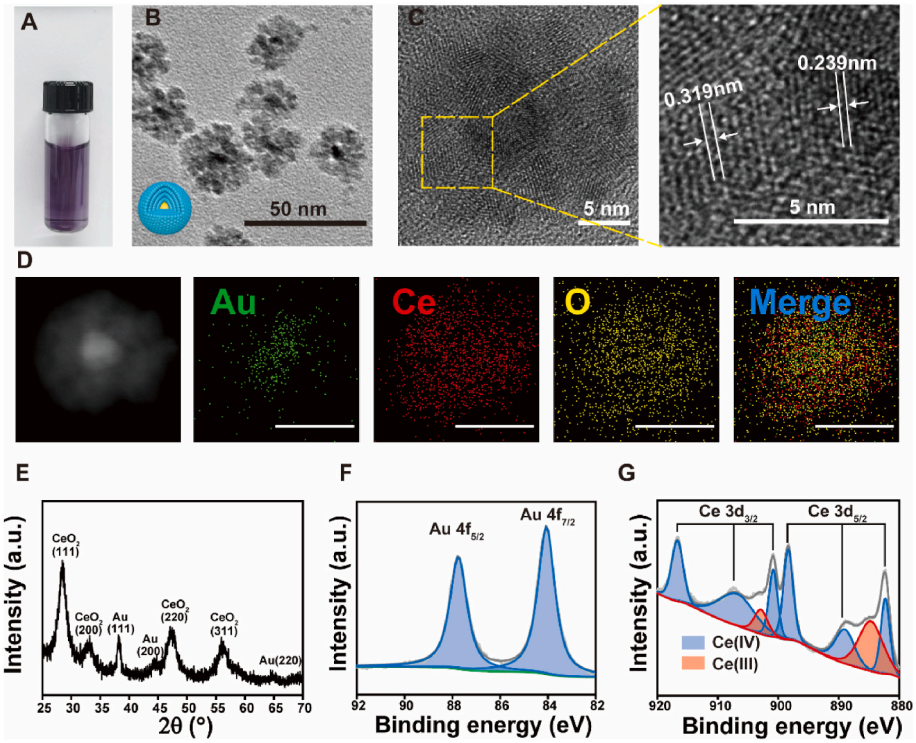

Fig. 1. Structure characterization of Au/CeO_2. (A) A photograph of Au/CeO_2 suspension. (B) TEM image of Au/CeO_2. Inset: a schematic image of Au/CeO_2. Scale bar, 50 nm. (C) HR-TEM image of Au/CeO_2. Scale bar, 5 nm. (D) STEM-EDX elemental maps of Au/CeO_2. Green for Au, red for Ce, and yellow for O. Scale bar, 20 nm. (E) XRD pattern of Au/CeO_2. (F) Au 4f XPS spectra of Au/CeO_2. (G) Ce 3d XPS spectra of Au/CeO_2.

collected from the mice receiving treatments. The length of the colons was measured. The colon tissues were fixed with 4% paraformaldehyde for hematoxylin and eosin (H&E) staining or frozen for cytokines examination.

To compare the therapeutic efficiency of Au/CeO_2@HA with 5-ASA, another animal experiment was performed. The colitis mice were induced as described above and were orally treated with Au/CeO_2@HA (2 mg/kg), CeO_2@HA (2 mg/kg), and 5-ASA (30 mg/kg) on predetermined time (day 7, day 9, and day 11). The body weights and disease activity index (DAI) of mice were recorded daily over the experimental period. The DAI was assigned scores as the literature [23]. On day 12, the entire colons were collected from the mice receiving treatments for colon length measurement and H&E staining.

2.14. Myeloperoxidase (MPO) activity measurement and enzyme linked immunosorbent assay (ELISA) analysis

To evaluate the inflammation level in mice, MPO activity and pro-inflammatory cytokines of the colon tissue isolated from the colitis mice receiving treatments were measured. The middle colon of each mouse was homogenized in RIPA lysis buffer (4 °C) [27]. Then, the resultant homogenate was centrifuged at 12000 rpm for 20 min at 4 °C, and the supernatant was collected for further detection. BCA assay was used to determine the protein concentration of the supernatant samples.

The MPO activity of colon tissues was measured as previously reported [48]. The supernatant (50 μL) was added to PBS (150 μL, pH 6.0, 50 mM) containing 0.2 mg/mL of *o*-dianisidine dihydrochloride and 0.005% H_2O_2 and incubated for 1 h. Next, the absorbance at 460 nm was recorded. The relative MPO activity was calculated by the following equation: relative MPO activity = A_{460}/C, where A_{460} is the absorbance at 460 nm of each sample, and C is the protein concentration of the supernatant samples.

Commercial mouse IL-6 ELISA kit (Biolegend, USA), TNF-α ELISA kit (Biolegend, USA), and IL-1β ELISA kit (KRISHGEN BioSystem, Indian) were used to quantify the amounts of IL-6, TNF-α, and IL-1β in the homogenate of colon tissues and serum according to the manufacturer's instructions. Briefly, the supernatant or serum (50 μL) was added into the wells that were pre-coated with the antibody of indicated pro-inflammatory cytokines and incubated for 2 h at room temperature. The residual sample was removed by the washing buffer. The detection antibody solution (100 μL) was added into the wells and incubated for 1 h at room temperature. After washing for 4 times, avidin-HRP solution (100 μL) was added into the wells and incubated for 30 min. Next, the plate was washed 5 times with washing buffer. Subsequently, substrate (100 μL) was added into the wells and incubated for 15 min in dark. Finally, the stop solution (100 μL) was mixed with the above substrates, and the absorbance at 450 nm was recorded. The concentrations of pro-inflammatory cytokines in colon tissues and serum were shown as pg/mg protein and pg/mL, respectively.

2.15. Statistical analysis

The significant difference was determined by the student's t-test. Statistically significant differences were defined as follows: *$p < 0.05$, **$p < 0.01$, ***$p < 0.001$, ns, not significant.

3. Result and discussion

3.1. Synthesis and characterization of Au/CeO_2

The Au/CeO_2 was synthesized through an auto-redox reaction between $AuCl_4^-$ and Ce^{3+} in the presence of ammonium hydroxide [44]. The synthesized Au/CeO_2 could be well dispersed in the aqueous solution with a characteristic absorption peak at 545 nm (Fig. 1A and **S1A)**. The transmission electron microscopy (TEM) images indicated that Au/CeO_2 displayed a core-shell nanostructure (22 nm, PDI: 0.03), and the Au core could be obviously observed in 92% of nanoparticles (Fig. 1B and S5A). High-resolution TEM (HR-TEM) images further

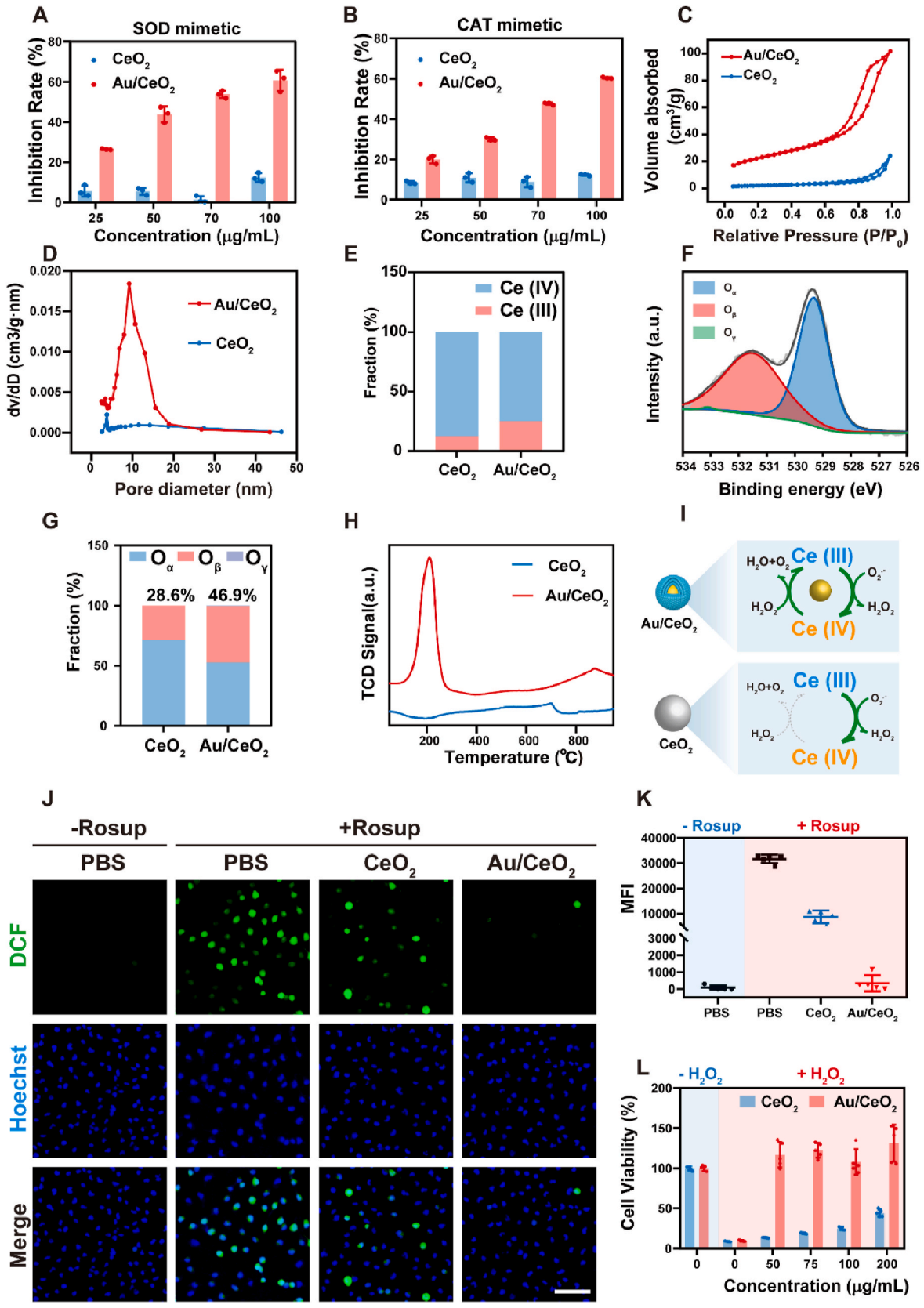

Fig. 2. ROS scavenging performance of Au/CeO_2 *in vitro*. (A) SOD-mimetic activities of Au/CeO_2 and CeO_2 ($n = 3$). (B) CAT-mimetic activities of Au/CeO_2 and CeO_2 ($n = 3$). (C) N_2 adsorption isotherms of Au/CeO_2 and CeO_2. (D) Pore size distributions of Au/CeO_2 and CeO_2. (E) Ce (III) and Ce (IV) fractions of Au/CeO_2 and CeO_2. (F) O 1s XPS spectrum of Au/CeO_2. (G) O_β fractions of Au/CeO_2 and CeO_2. (H) Temperature-programmed reduction of H_2 curves. (I) Schematic illustration of enhanced catalytic activity of Au/CeO_2. (J) Representative ROS staining and relative mean fluorescence intensity (K) of NCM460 cells in the presence of Rosup and Au/CeO_2 or CeO_2. Scale bar, 100 μm. (L) Viabilities of NCM460 cells in the presence of H_2O_2 and Au/CeO_2 ($n = 5$). Data represent mean ± SD.

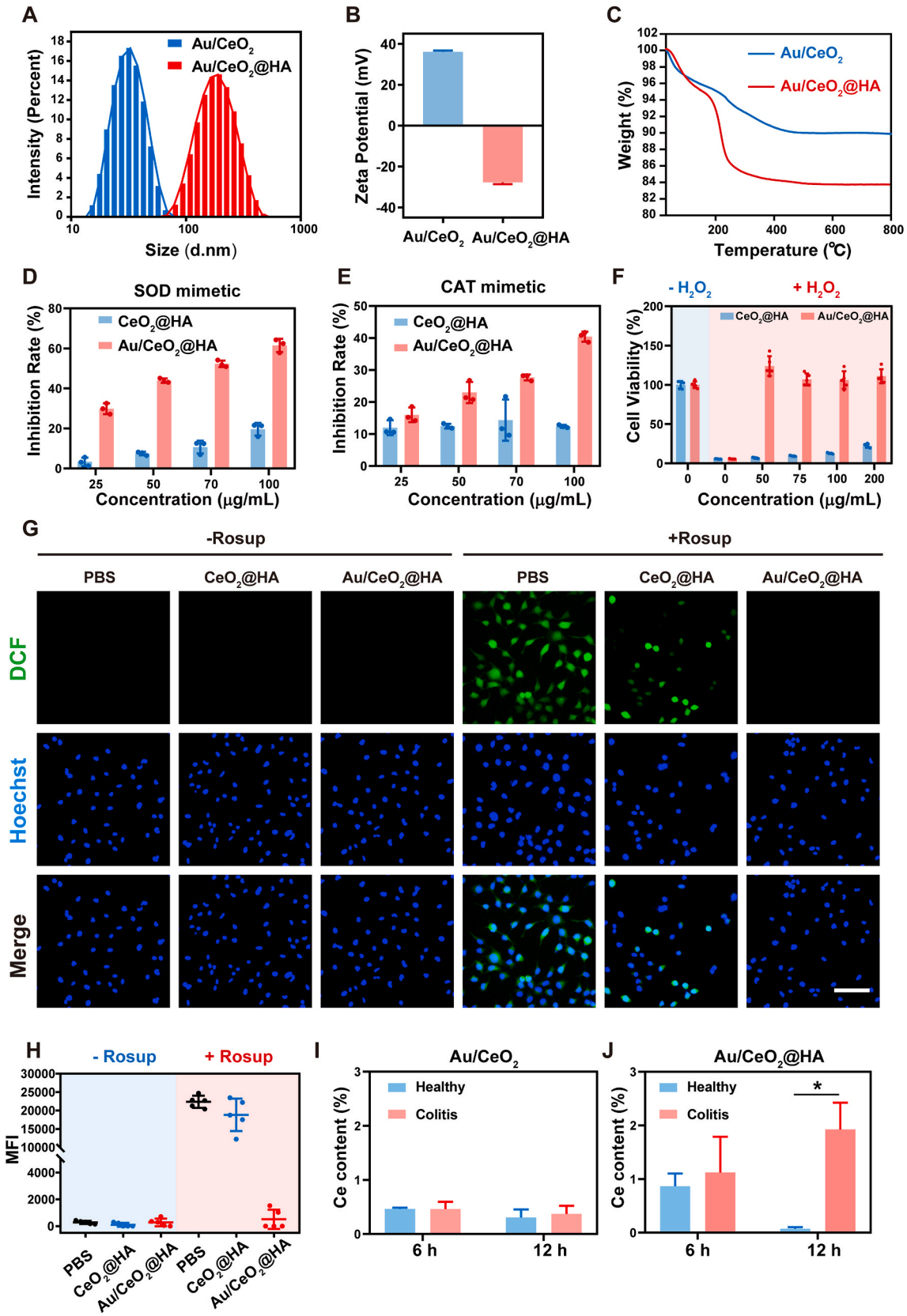

Fig. 3. Modification Au/CeO_2 with HA. (A) DLS size distribution of Au/CeO_2 and Au/CeO_2@HA. (B) Zeta potentials of Au/CeO_2 and Au/CeO_2@HA. (C) TGA curves of Au/CeO_2 and Au/CeO_2@HA. (D) SOD mimics activities of Au/CeO_2@HA and CeO_2@HA ($n = 3$). (E) CAT mimics activities of Au/CeO_2@HA and CeO_2@HA ($n = 3$). (F) Relative viability of NCM460 cells under H_2O_2-treatment in the presence of Au/CeO_2@HA ($n = 5$). (G) Representative ROS staining and (H) relative mean fluorescence intensity of NCM460 cells under Rosup-treatment. Blue: Hoechst, and green: DCF ($n = 9$). Scale bar, 100 μm. (I–J) Relative Ce contents in the colonic tissues of mice after treating with Au/CeO_2 (I) or Au/CeO_2@HA (J) orally. Data represent mean ± SEM.

revealed the lattice distance of shell corresponding to the (111) planes of CeO_2 (0.319 nm) and the lattice distance of core corresponding to the (111) planes of Au (0.239 nm) (Fig. 1C). Moreover, the energy-dispersive X-ray spectroscopy (EDX) element mappings confirmed that the Au elements were mainly distributed in the core of nanoparticles, while the Ce and O elements exhibited uniform distributions (Fig. 1D). The crystalline feature of Au/CeO_2 was characterized by an X-ray powder diffraction (XRD) pattern, indicating the characteristic peaks of CeO_2 (JCPDS No.34-0394) and Au (JCPDS No.04-0784) (Fig. 1E). To further examine the composition and valence states, X-ray photoelectron spectroscopy (XPS) was employed to characterize the Au/CeO_2. The two peaks in Au 4f spectrum were consistent with Au (0) (Fig. 1F), and the Ce 3d spectrum revealed the co-existence of Ce (III) and Ce (IV) oxidation states in ceria (Fig. 1G). All these results indicate that Au/CeO_2 nanoparticles are successfully synthesized, and the CeO_2 is formed on the outer shell while the Au NP is encapsulated in the core.

3.2. Enhanced antioxidant enzymatic activity of Au/CeO_2

The ROS eliminating capacity of Au/CeO_2 was investigated towards superoxide anions ($O_2^{\bullet-}$) and hydrogen peroxide (H_2O_2), and the commercial CeO_2 was chosen as a control. The SOD-like catalytic activity ($O_2^{\bullet-}$ scavenging) of these nanozymes was studied using the water-soluble tetrazolium 1 (WST-1) method (Fig. 2A). The Au/CeO_2 efficiently eliminated the $O_2^{\bullet-}$ in a dose-dependent manner, and scavenged over 60% of $O_2^{\bullet-}$ at the concentration of 100 μg/mL within 20 min. In sharp contrast, the commercial CeO_2 exhibited limited efficiency on $O_2^{\bullet-}$ clearance at all the tested concentrations (25–100 μg/mL). Next, the CAT-like catalytic activity was investigated by determining H_2O_2 scavenging (Fig. 2B). Similarly, Au/CeO_2 exhibited dramatically higher H_2O_2 eliminating efficacy compared with commercial CeO_2. Furthermore, kinetics analysis was performed and the results fitted the Michaelis−Menten kinetics. The Michaelis-Menten constant (K_m) value and CAT-like activity of Au/CeO_2 were calculated to be 3.224 mM and 6.330 U/mg, respectively (Figs. S2A and S2B). These results indicate that Au/CeO_2 possesses multi-enzymatic activities for eliminating both $O_2^{\bullet-}$ and H_2O_2, which are markedly higher than that of its commercial counterpart. Moreover, we synthesized two types of CeO_2 nanoparticles as the previous studies [27,43], and found that Au/CeO_2 also exhibited higher ROS scavenging efficacy compared with these ceria nanoparticles (Figs. S2C and S2D), confirming the good antioxidant activity of Au/CeO_2.

The catalytic efficacy is highly dependent on the exposed active sites of nanozymes. Thus, nitrogen adsorption isotherms analysis was performed to investigate the surface-to-volume ratio. The Brunauer-Emmett-Teller (BET) surface area of Au/CeO_2 was about 10-fold higher than that of CeO_2 (Fig. 2C), and the mesopores (5–20 nm) could be detected in Au/CeO_2 (Fig. 2D), which formed by the stacking of CeO_2 around Au core [44]. The high surface-to-volume and large void in the core-shell structure of Au/CeO_2 would sufficiently expose the catalytic sites to facilitate interactions between ROS and nanozymes. Moreover, the valence ratio of Ce (III)/Ce (IV) and oxygen species also plays essential roles in the catalytic activity of ceria nanoparticles. Both Au/CeO_2 and commercial CeO_2 possessed dual oxidation states of Ce (Fig. 1G and S1C), but the ratio of Ce (III)/Ce (IV) in Au/CeO_2 (25.1/74.9) was twice as high as that in CeO_2 (12.7/87.3) (Fig. 2E). The O1s spectra revealed the characteristic peaks of lattice oxygen (O_α), surface oxygen species (O_β), and chemisorbed water and/or carbonated (O_γ) (Fig. 2F and G, and S1D). Among them, O_β from defective sites was reported to play a significant role in most catalytic progress [49]. Quantitative analysis suggests that the increased Ce (III) promotes O_β percentage in Au/CeO_2 (46.9%) compared to CeO_2 (28.6%) (Fig. 2G). The rate of reduction from Ce (IV) to Ce (III) was also a crucial challenge for the regeneration of enzyme-mimic activity of ceria nanoparticles [43,50]. Thus, the temperature-programmed reduction (TPR) analysis was performed. In the H_2-TPR spectrum of Au/CeO_2, a reduction peak was observed at 210 °C, which was significantly lower than the reported reduction temperature of ceria nanoparticles (398 °C) [43], while no significant reduction peak appeared in the spectrum of commercial CeO_2 (Fig. 2H). The decreased reduction temperature might be induced by the accelerated electron transfer by the Au nanocore in Au/CeO_2 and the great reducing capability of Au–H species on the surface of Au nanocore [44,51]. These results suggest that Au/CeO_2 not only possesses higher contents of Ce (III) and oxygen vacancy but also accelerates the reduction from Ce (IV) to Ce (III) compared with commercial CeO_2, thus resulting in enhanced catalytic activities of Au/CeO_2 (Fig. 2I).

Encouraged by the excellent antioxidant activity, NCM460 cells were employed to assess the cellular ROS eliminating capability of Au/CeO_2. In the presence of Rosup, a ROS-generated reagent, the intracellular ROS was significantly elevated in NCM460 cells with obviously green fluorescence indicated by 2′, 7’ –dichlorofluorescein (DCF) (Fig. 2J). The Au/CeO_2 entered into the cells and mainly localized in the lysosomes (Fig. S3A), and sufficiently eliminated the overproduced ROS by 99.2% in Rosup-treated cells, of which the intracellular ROS level was as low as the untreated cells (Fig. 2J and K), while CeO_2 only scavenged 72.8% of ROS. Due to the excellent ROS elimination efficacy, Au/CeO_2 almost abrogated the damage induced by oxidative stress and recovered the cell viability of H_2O_2-treated cells (Fig. 2L). In contrast, CeO_2 only elevated the cell viability to 44% at the high concentration of 200 μg/mL, likely because of its limited antioxidant activity. Taken together, these results indicate that the Au/CeO_2 with excellent enzymatic activities could sufficiently scavenge ROS to protect cells from oxidative stress.

3.3. HA modification on Au/CeO_2 enhances specific accumulation in inflamed colons

The depletion and discontinuity of mucus layer [52], accumulation of positively charged proteins (including transferrin [53], bacteriostatic [54], and eosinophil cationic protein [55]) at inflammatory sites, and overexpressed CD44 on inflamed epithelial cells [56–58] are the prominent features of colitis. Hyaluronic acid (HA), an anionic natural polysaccharide with a specific affinity of CD44, would be an ideal target group for inflammatory intestinal through electrostatic and HA-CD44 interactions [48,59]. To promote the specific accumulation of Au/CeO_2 toward the inflammation site, dopamine-grafted HA was employed to modify the positively-charged Au/CeO_2 via electrostatic interaction.

After HA modification on Au/CeO_2, the hydrodynamic diameter of nanoparticles increased from 30.4 nm to 160 nm likely due to forming clusters (Fig. 3A and **S5A)**, and the zeta-potential reversed from positive (+36.1 mV) to negative (−27.7 mV) (Fig. 3B), while the UV–Vis spectrum was hardly changed by HA coating (Fig. S1A). Moreover, the weight loss of HA-coated nanoparticles (Au/CeO_2@HA) increased by 6.3% in thermogravimetric analysis (TGA) compared to Au/CeO_2 (Fig. 3C). These results revealed that Au/CeO_2 was successfully modified with HA. As a control, the CeO_2 was also modified with HA (Figs. S6A–C). Of note, the HA modification on Au/CeO_2 had a negligible influence on the SOD mimetic activity (Fig. 3D) and slightly reduced the CAT-like activity (Fig. 3E), which was much higher than that of CeO_2@HA. Hence, Au/CeO_2@HA sufficiently eliminated the intracellular ROS and protected cells from H_2O_2-induced damages, while CeO_2@HA hardly weakened the oxidative stress *in vitro* (Fig. 3F–H and S3B**)**. These results indicate that HA modification maintained the excellent ROS-scavenging activity and cytoprotection ability of Au/CeO_2. Importantly, the relative catalytic activity of Au/CeO_2@HA remained higher than 85% after incubation with simulated gastric fluid (SGF) for 4 h or simulated intestinal fluid (SIF) for 72 h, and the hydrodynamic size and zeta potential were just decreased slightly after treatments (Figs. S5B–S5E), suggesting the good stability of Au/CeO_2@HA.

Next, we suspected the HA coating on Au/CeO_2 would facilitate the retention in inflamed colon tissues due to the HA-CD44 mediated

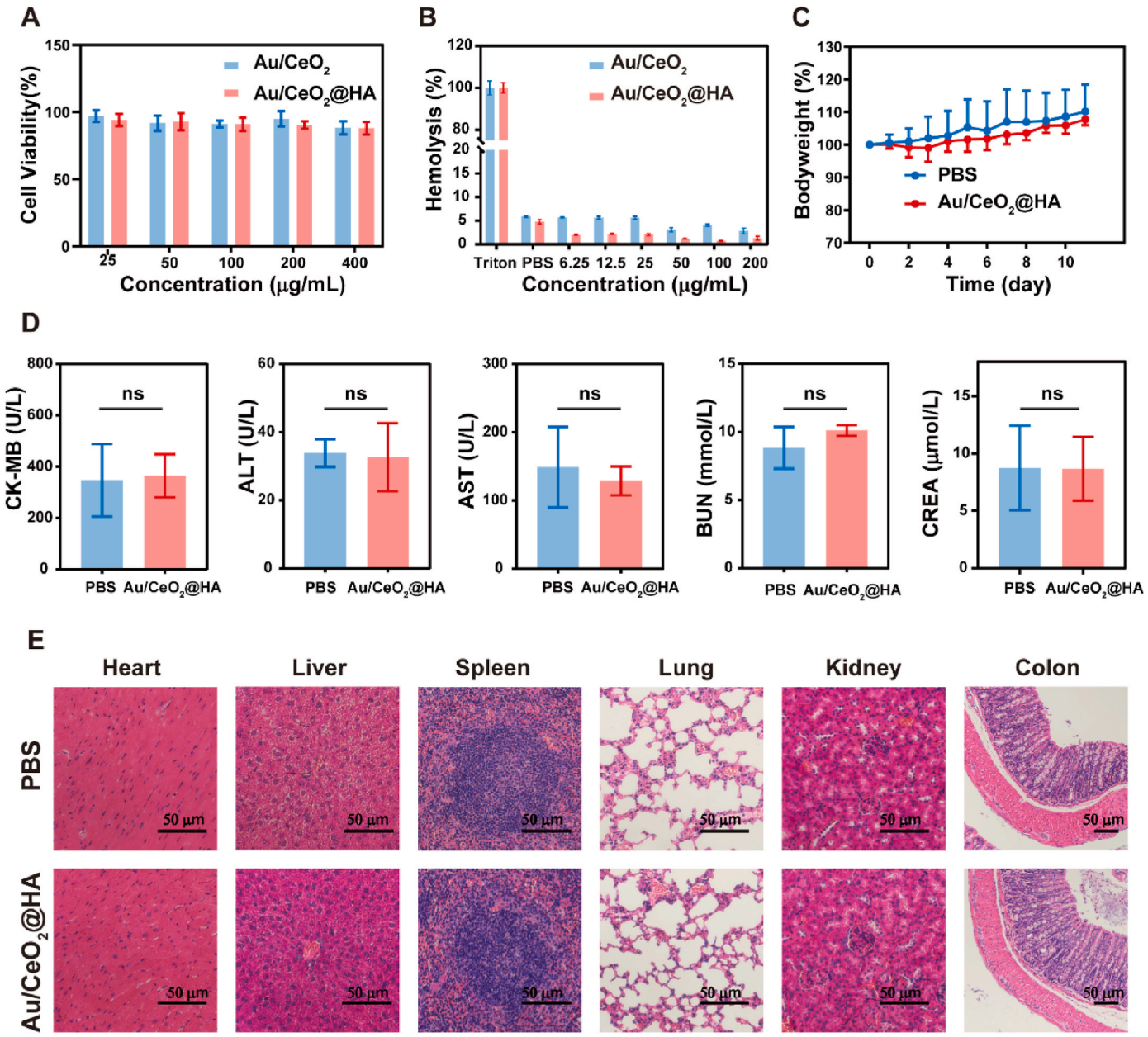

Fig. 4. Biosafety of Au/CeO_2@HA. (A) Cell viabilities of NCM460 cells after incubation with Au/CeO_2 or Au/CeO_2@HA ($n = 5$). (B) Hemolysis activity of Au/CeO_2 and Au/CeO_2@HA. ($n = 3$) (C) Relative body weights of healthy mice receiving Au/CeO_2@HA treatment (2 mg/kg, oral administration, three times) ($n = 5$). (D) Analysis of main biochemical indexes in serum ($n = 5$). (E) Hematoxylin-eosin (H&E) staining of the major organs from mice receiving Au/CeO_2@HA treatment. Scale bars, 50 μm.

interaction and the electrostatic interaction. To test this notion, the healthy and acute colitis (induced by dextran sulfate sodium (DSS)) mice were treated with Au/CeO_2 and Au/CeO_2@HA (by oral, 2 mg/kg), respectively. Six or 12 h after treatment, the colon tissues were isolated for testing nanoparticle accumulation by determining the Ce contents using ICP-MS. Six hours after treatment, Au/CeO_2@HA was detected in both healthy colons and colitis colons. For the positively-charged Au/CeO_2, the Ce accumulation exhibited no significant difference in health and colitis colons (Fig. 3I). On the contrary, Au/CeO_2@HA effectively accumulated in the inflamed colon tissues at 12 h post-treatment, which was almost eliminated from the healthy colons at this time (Fig. 3J). Notably, the Ce content in the colons of colitis mice receiving Au/CeO_2@HA was significantly higher (5.2-fold) than that of colitis mice receiving Au/CeO_2 (Fig. S7A). These Au/CeO_2@HA nanoparticles could be gradually excreted and almost eliminated from the colons in colitis mice after 72 h (Figs. S7B and S9A), which would not induce long term accumulation. These results indicate that the HA coating specifically enhances ceria nanozyme accumulation in inflamed colon tissues and maintained catalytic activities.

3.4. Biocompatibility of Au/CeO_2@HA

Biocompatibility is a prerequisite for nanomedicine. Thus, the potential toxicity of Au/CeO_2@HA was investigated before therapeutic study *in vivo*. To test *in vitro* biocompatibility, the cytotoxicity and hemolysis activity were studied. The viability of NCM460 cells exposed to Au/CeO_2@HA was higher than 88% even at the concentration up to 400 μg/mL (Fig. 4A), and no obvious hemolysis was observed at all the test concentrations (Fig. 4B and Fig. S8). Of note, the hemolysis rate slightly decreased by HA-coating likely due to the surface charge reversal of

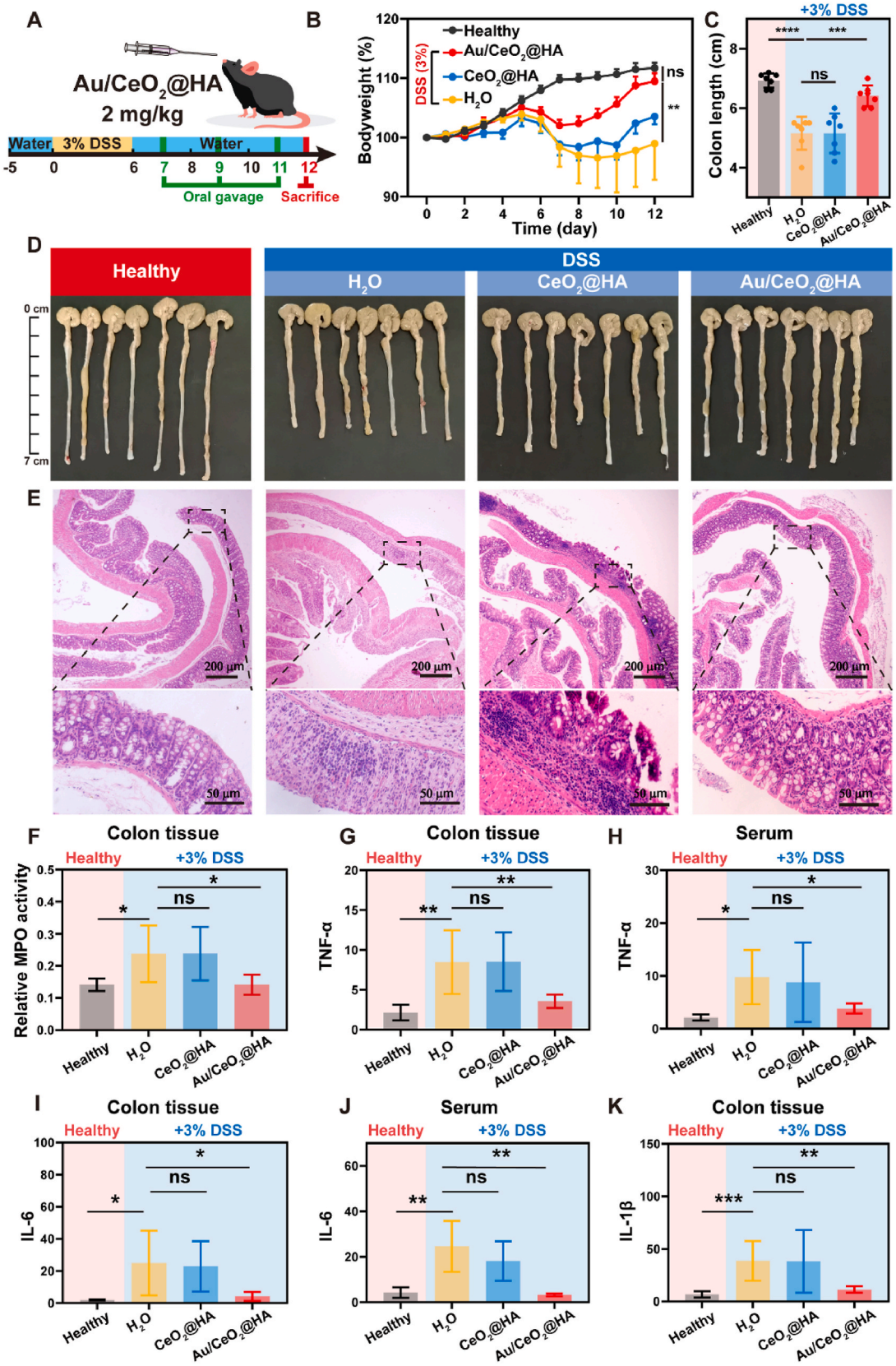

Fig. 5. Therapeutic effect of Au/CeO_2@HA in ulcerative colitis. (A) Overall protocol of the animal experiment. C57BL/6 mice received water or 3% DSS-containing water for 6 consecutive days. On the day 7, 9, and 11, mice were orally administered with Au/CeO_2@HA or CeO_2@HA (2 mg/kg) ($n = 7$). (B) Relative body weights of mice receiving treatments. (C) Colon lengths and (D) photos of colon tissues with indicated treatments on day 12. (E) Hematoxylin-eosin (H&E) staining images of colon tissues. (F) Relative myeloperoxidase (MPO) activity in colon homogenates. TNF-α levels in colon homogenates (G) and serum (H) of each group. IL-6 levels in colon homogenates (I, pg/mg protein) and serum (J, pg/mL) of each group. (K) IL-1β levels in colon homogenates of each group. Data represent mean ± SD (*$p < 0.05$, **$p < 0.01$, and ***$p < 0.001$).

nanoparticles. Next, the healthy C57BL/6 mice were treated with Au/CeO_2@HA via oral administration (3 times, 2 mg/kg). The body weights of mice were not affected by Au/CeO_2@HA treatment as well as healthy mice (Fig. 4C). Moreover, the main biochemical indicators of serum reflecting the functions of the heart (CK-MB), liver (ALT, AST), and kidney (BUN, CREA) were not markedly changed by Au/CeO_2@HA treatment (Fig. 4D), suggesting that Au/CeO_2@HA does not affect the functions of major organs. Consistently, no significant difference was observed in the hematoxylin-eosin (H&E) staining images of the organs (heart, liver, spleen, lung, kidney, and colon) between Au/CeO_2@HA group and untreated mice (Fig. 4E). These results illustrated that Au/CeO_2@HA treatment did not damage the major organs and affect their functions, suggesting the good biocompatibility of Au/CeO_2@HA *in vivo*.

3.5. Therapeutic effects of Au/CeO_2@HA in DSS-induced acute colitis

Based on the excellent ROS-scavenging ability and biocompatibility, the therapeutic effect of Au/CeO_2@HA was tested in the acute ulcerative colitis model induced by DSS (Fig. 5A). The body weights of colitis mice receiving DSS for 6 days decreased significantly (Fig. 5B), indicating the successful establishment of the colitis model. In contrast to colitis mice receiving water with irrevocably decreased body weights, Au/CeO_2@HA promptly stopped the weight loss on day 8 and recovered the body weights of colitis mice to the level of healthy mice on day 12 (Fig. 5B). Moreover, Au/CeO_2@HA treatment sufficiently abrogated the shortening of colon length (Fig. 5C and D, and Fig. S9B), which is a characteristic feature of colon injury induced by muscle wasting associated with inflammation progression [60]. However, CeO_2@HA was completely ineffective to alleviate the weight loss and colon shortening. Similar to the colons of colitis mice showing severe disorder of intestinal structure, including crypt disappearance, significantly loose goblet cells, and inflammatory cell infiltration (Fig. 5E), the colitis mice treated with CeO_2@HA still suffered from crypt atrophy and inflammatory cell infiltration. In stark contrast, the colon structure of mice receiving Au/CeO_2@HA was preserved as well as the healthy mice (Fig. 5E). Moreover, the therapeutic effect of Au/CeO_2@HA was confirmed by comparing it with 5-amino salicylic acid (5-ASA), a clinically used therapeutic agent for colitis (Fig. S10). Consistently, Au/CeO_2@HA sufficiently alleviated the colon damage and recovered the body weight and colon length of colitis mice, while 5-ASA exhibited limited therapeutic efficacy likely due to its poor availability [61,62].

To further investigate the therapeutic effect of Au/CeO_2@HA, myeloperoxidase (MPO) and typical pro-inflammatory cytokines were measured. MPO is a unique granule heme enzyme of neutrophils and monocytes, which can produce powerful ROS, especially hypochlorous acid (HOCl) [63]. The upregulated HOCl not only induces cell apoptosis, but also exacerbates the inflammatory response [63–65]. Compared with healthy colon tissues, DSS feeding dramatically elevated the MPO activity. Such enhanced MPO activity induced by DSS was effectively downregulated by Au/CeO_2@HA to the level as low as that of healthy colons (Fig. 5F). Similarly, the pro-inflammatory cytokines (IL-1β, IL-6, and TNF-α) in colon tissue and serum were also increased by DSS, which were normalized by Au/CeO_2@HA treatment (Fig. 5G–K). Taken together, these results demonstrate that the Au/CeO_2@HA could effectively alleviate DSS-induced colitis by reducing infiltration of inflammatory cells and pro-inflammatory cytokines production.

4. Conclusion

In summary, we developed a gold nanoparticle-embedded ceria nanozyme (Au/CeO_2) with ROS-scavenging activities for treating ulcerative colitis. The Au/CeO_2 exhibited significantly enhanced enzymatic catalytic activities (SOD and CAT) compared with the commercial ceria, likely due to the porous structure and fast reduction rate from cerium (IV) to cerium (III) induced by the gold core. After being coated with hyaluronic acid (HA), the negatively-charged Au/CeO_2@HA could sufficiently accumulate in the inflamed colon tissues and inherit excellent catalytic activities for eliminating ROS ($O_2^{\bullet-}$ and H_2O_2). In the DSS-induced colitis, Au/CeO_2@HA effectively recovered the body weight and colon length of colitis mice by reducing the infiltration of inflammatory cells and the production of proinflammatory cytokines, while the HA-coated commercial ceria (CeO_2@HA) hardly alleviated the colitis. Thus, this work not only demonstrated a versatile method to facilitate the catalytic activity of ceria but also provided an excellent antioxidant nanotherapeutic for treating colitis.

Ethics approval and consent to participate

All the animal experiments were performed following the guideline approved by the Institution Animal Care and Use Committee (IACUC) at Tongji Medical College, Huazhong University of Science and Technology, Wuhan, China (IACUC Number: 2674).

CRediT authorship contribution statement

Mingyi Li: contributed equally to this work. designed experiments, Data curation, performed the experiments and collected data, Writing – original draft, Writing – review & editing. **Jia Liu:** contributed equally to this work, Supervisiondesigned and supervised the work, designed experiments, Data curation, Writing – original draft, Writing – review & editing. **Lin Shi:** helped with animal experiments. **Cheng Zhou:** helped with animal experiments. **Meizhen Zou:** Writing – review & editing. **Daan Fu:** helped with animal experiments. **Ye Yuan:** helped with animal experiments. **Chundong Yao:** helped with animal experiments. **Lifang Zhang:** helped with animal experiments. **Sumei Qin:** helped with animal experiments. **Miaodeng Liu:** helped with characterization and software. **Qian Cheng:** helped with characterization and software. **Zheng Wang:** Supervisiondesigned and supervised the work, Writing – original draft, Writing – review & editing. **Lin Wang:** Supervisiondesigned and supervised the work, Writing – original draft, Writing – review & editing.

Declaration of competing interest

The authors declare that they have no known competing financial interests or personal relationships that could have appeared to influence the work reported in this paper.

Acknowledgments

This work was supported by the National Natural Science Foundation of China (82072068, 82072167, 81873931, and 81974382), the Integrated Innovative Team for Major Human Diseases Program of Tongji Medical College of HUST, the Academic Doctor Supporting Program of Tongji Medical College, HUST, the Knowledge Innovation Special Project for Fundamental Research of Wuhan (2022020801010461), the Union Hospital Foundation for Young Scientist (2021xhqh01), and the Open Foundation of Hubei Key Laboratory of Regenerative Medicine and Multi-disciplinary Translational Research (2022zsyx001). All the animals used in this study were housed under specific pathogen-free conditions in the animal center of Tongji Medical College, Huazhong University of Science and Technology.

Appendix A. Supplementary data

Supplementary data to this article can be found online at https://doi.org/10.1016/j.bioactmat.2023.01.015.

References

[1] C.N. Bernstein, M. Fried, J.H. Krabshuis, H. Cohen, R. Eliakim, S. Fedail, R. Gearry, K.L. Goh, S. Hamid, A.G. Khan, A.W. LeMair, Malfertheiner, Q. Ouyang, J.F. Rey,

A. Sood, F. Steinwurz, O.O. Thomsen, A. Thomson, G. Watermeyer, World gastroenterology organization practice guidelines for the diagnosis and management of IBD in 2010, Inflamm. Bowel Dis. 16 (1) (2010) 112–124.
[2] M.L. Hoivik, B. Moum, I.C. Solberg, M. Henriksen, M. Cvancarova, T. Bernklev, I. Group, Work disability in inflammatory bowel disease patients 10 years after disease onset: results from the IBSEN Study, Gut 62 (3) (2013) 368–375.
[3] D.C. Baumgart, W.J. Sandborn, Inflammatory bowel disease: clinical aspects and established and evolving therapies, Lancet 369 (9573) (2007) 1641–1657.
[4] C.M. Olesen, M. Coskun, L. Peyrin-Biroulet, O.H. Nielsen, Mechanisms behind efficacy of tumor necrosis factor inhibitors in inflammatory bowel diseases, Pharmacol. Ther. 159 (2016) 110–119.
[5] A. Stallmach, S. Hagel, T. Bruns, Adverse effects of biologics used for treating IBD, Best Pract. Res. Clin. Gastroenterol. 24 (2) (2010) 167–182.
[6] R.P. Hirten, M. Iacucci, S. Shah, S. Ghosh, J.F. Colombel, Combining biologics in inflammatory bowel disease and other immune mediated inflammatory disorders, Clin. Gastroenterol. Hepatol. 16 (9) (2018) 1374–1384.
[7] S.P. Colgan, C.T. Taylor, Hypoxia: an alarm signal during intestinal inflammation, Nat. Rev. Gastroenterol. Hepatol. 7 (5) (2010) 281–287.
[8] M. Iborra, I. Moret, F. Rausell, G. Bastida, M. Aguas, E. Cerrillo, P. Nos, B. Beltran, Role of oxidative stress and antioxidant enzymes in Crohn's disease, Biochem. Soc. Trans. 39 (4) (2011) 1102–1106.
[9] M.A. Alzoghaibi, Concepts of oxidative stress and antioxidant defense in Crohn's disease, World J. Gastroenterol. 19 (39) (2013) 6540–6547.
[10] Y. Naito, T. Takagi, T. Yoshikawa, Molecular fingerprints of neutrophil-dependent oxidative stress in inflammatory bowel disease, J. Gastroenterol. 42 (10) (2007) 787–798.
[11] L. Lih-Brody, S.R. Powell, K.P. Collier, G.M. Reddy, R. Cerchia, E. Kahn, G. S. Weissman, S. Katz, R.A. Floyd, M.J.J. McKinley, Increased oxidative stress and decreased antioxidant defenses in mucosa of inflammatory bowel disease, Dig. Dis. Sci. 41 (10) (1996) 2078–2086.
[12] A. Roessner, D. Kuester, P. Malfertheiner, R. Schneider-Stock, Oxidative stress in ulcerative colitis-associated carcinogenesis, Pathol. Res. Pract. 204 (7) (2008) 511–524.
[13] A. Rezaie, R.D. Parker, M. Abdollahi, Oxidative stress and pathogenesis of inflammatory bowel disease: an epiphenomenon or the cause? Dig. Dis. Sci. 52 (9) (2007) 2015–2021.
[14] I.E. Koutroubakis, N. Malliaraki, P.D. Dimoulios, K. Karmiris, E. Castanas, E.A. J. Kouroumalis, Decreased total and corrected antioxidant capacity in patients with inflammatory bowel disease, Dig. Dis. Sci. 49 (9) (2004) 1433–1437.
[15] A. Bhattacharyya, R. Chattopadhyay, S. Mitra, S.E. Crowe, Oxidative stress: an essential factor in the pathogenesis of gastrointestinal mucosal diseases, Physiol. Rev. 94 (2) (2014) 329–354.
[16] T.T. Jubeh, M. Nadler-Milbauer, Y. Barenholz, A. Rubinstein, Local treatment of experimental colitis in the rat by negatively charged liposomes of catalase, TMN and SOD, J. Drug Target. 14 (3) (2006) 155–163.
[17] K.E. Barrett, D.F. McCole, Hydrogen peroxide scavenger, catalase, alleviates ion transport dysfunction in murine colitis, Clin. Exp. Pharmacol. Physiol. 43 (11) (2016) 1097–1106.
[18] Y. Suzuki, T. Matsumoto, S. Okamoto, T. Hibi, A lecithinized superoxide dismutase (PC-SOD) improves ulcerative colitis, Colorectal Dis. 10 (9) (2008) 931–934.
[19] S. Ramasamy, D.D. Nguyen, M.A. Eston, S.N. Alam, A.K. Moss, F. Ebrahimi, B. Biswas, G. Mostafa, K.T. Chen, K. Kaliannan, H. Yammine, S. Narisawa, J. L. Millan, H.S. Warren, E.L. Hohmann, E. Mizoguchi, H.C. Reinecker, A.K. Bhan, S. B. Snapper, M.S. Malo, R.A. Hodin, Intestinal alkaline phosphatase has beneficial effects in mouse models of chronic colitis, Inflamm. Bowel Dis. 17 (2) (2011) 532–542.
[20] J. Bilski, A. Mazur-Bialy, D. Wojcik, J. Zahradnik-Bilska, B. Brzozowski, M. Magierowski, T. Mach, K. Magierowska, T. Brzozowski, The role of intestinal alkaline phosphatase in inflammatory disorders of gastrointestinal tract, Mediat. Inflamm. 2017 (2017), 9074601.
[21] Y. Lin, J. Ren, X. Qu, Catalytically active nanomaterials: a promising candidate for artificial enzymes, Acc. Chem. Res. 47 (4) (2014) 1097–1105.
[22] L. Hou, F. Gong, B. Liu, X. Yang, L. Chen, G. Li, Y. Gong, C. Liang, N. Yang, X. Shen, Z. Liu, L. Cheng, Orally administered titanium carbide nanosheets as anti-inflammatory therapy for colitis, Theranostics 12 (8) (2022) 3834–3846.
[23] Z. Jiulong, C. Xiaojun, G. Wei, Z. Linlin, Z. Duowu, Z. Yuanyi, L. Zhaoshen, C. Hangrong, Prussian blue nanozyme with multienzyme activity reduces colitis in mice, ACS Appl. Mater. Interfaces 10 (31) (2018) 26108–26117.
[24] Z. Jiulong, G. Wei, C. Xiaojun, X. Jiajia, Z. Duowu, L. Zhaoshen, H. Bing, Z. Yuanyi, Nanozyme-mediated catalytic nanotherapy for inflammatory bowel disease, Theranostics 9 (10) (2019) 2843–2855.
[25] L. Yufeng, C. Yuan, Z. He, Z. Min, Y. Yijun, L. Shichao, J. Bo, Z. Xiaozhi, M. Leiying, W. Chuan-Wan, L. Quanyi, L. Ying-Wu, D. Yan, J.B. Christopher, W. Hui, Integrated cascade nanozyme catalyzes in vivo ROS scavenging for anti-inflammatory therapy, Sci. Adv. 6 (29) (2020), eabb2695.
[26] C. Yuan, C. Chaoqun, Y. Jia, Y. Yijun, L. Yufeng, Z. He, M. Leiying, W. Hui, Mn_3O_4 nanozyme for inflammatory bowel disease therapy, Adv. Ther. 4 (9) (2021), 2100081.
[27] S. Zhao, Y. Li, Q. Liu, S. Li, Y. Cheng, C. Cheng, Z. Sun, Y. Du, C.J. Butch, H. Wei, An orally administered CeO_2@Montmorillonite nanozyme targets inflammation for inflammatory bowel disease therapy, Adv. Funct. Mater. 30 (45) (2020), 2004692.
[28] N. Zhao, F.E. Yang, C.Y. Zhao, S.W. Lv, J. Wang, J.M. Liu, S. Wang, Construction of pH-dependent nanozymes with oxygen vacancies as the high-efficient reactive oxygen species scavenger for oral-administrated anti-inflammatory therapy, Adv. Healthcare Mater. 10 (23) (2021), e2101618.
[29] A. Yuan, F. Xia, Q. Bian, H. Wu, Y. Gu, T. Wang, R. Wang, L. Huang, Q. Huang, Y. Rao, D. Ling, F. Li, J. Gao, Ceria nanozyme-integrated microneedles reshape the perifollicular microenvironment for androgenetic alopecia treatment, ACS Nano 15 (8) (2021) 13759–13769.
[30] D. Ni, H. Wei, W. Chen, Q. Bao, Z.T. Rosenkrans, T.E. Barnhart, C.A. Ferreira, Y. Wang, H. Yao, T. Sun, D. Jiang, S. Li, T. Cao, Z. Liu, J.W. Engle, P. Hu, X. Lan, W. Cai, Ceria nanoparticles meet hepatic ischemia-reperfusion injury: the perfect imperfection, Adv. Mater. 31 (40) (2019), e1902956.
[31] F. Li, Y. Qiu, F. Xia, H. Sun, H. Liao, A. Xie, J. Lee, P. Lin, M. Wei, Y. Shao, B. Yang, Q. Weng, D. Ling, Dual detoxification and inflammatory regulation by ceria nanozymes for drug-induced liver injury therapy, Nano Today 35 (2020), 100925.
[32] K. Wang, Y. Zhang, W. Mao, W. Feng, S. Lu, J. Wan, X. Song, Y. Chen, B. Peng, Engineering ultrasmall ferroptosis-targeting and reactive oxygen/nitrogen species-scavenging nanozyme for alleviating acute kidney injury, Adv. Funct. Mater. 32 (10) (2021), 2109221.
[33] Q. Chen, Y. Du, K. Zhang, Z. Liang, J. Li, H. Yu, R. Ren, J. Feng, Z. Jin, F. Li, J. Sun, M. Zhou, Q. He, X. Sun, H. Zhang, M. Tian, D. Ling, Tau-Targeted multifunctional nanocomposite for combinational therapy of alzheimer's disease, ACS Nano 12 (2) (2018) 1321–1338.
[34] H.J. Kwon, M.Y. Cha, D. Kim, D.K. Kim, M. Soh, K. Shin, T. Hyeon, I. Mook-Jung, Mitochondria-targeting ceria nanoparticles as antioxidants for alzheimer's disease, ACS Nano 10 (2) (2016) 2860–2870.
[35] Q. Bao, P. Hu, Y. Xu, T. Cheng, C. Wei, L. Pan, J. Shi, Simultaneous blood-brain barrier crossing and protection for stroke treatment based on edaravone-loaded ceria nanoparticles, ACS Nano 12 (7) (2018) 6794–6805.
[36] E. Casals, M. Zeng, M. Parra-Robert, G. Fernandez-Varo, M. Morales-Ruiz, W. Jimenez, V. Puntes, G. Casals, Cerium oxide nanoparticles: advances in biodistribution, toxicity, and preclinical exploration, Small 16 (20) (2020), 1907322.
[37] M.S. Lord, J.F. Berret, S. Singh, A. Vinu, A.S. Karakoti, Redox active cerium oxide nanoparticles: current status and burning issues, Small 17 (51) (2021), e2102342.
[38] I. Celardo, J.Z. Pedersen, E. Traversa, L. Ghibelli, Pharmacological potential of cerium oxide nanoparticles, Nanoscale 3 (4) (2011) 1411–1420.
[39] I. Celardo, M. De Nicola, C. Mandoli, J.Z. Pedersen, E. Traversa, L. Ghibelli, Ce^{3+} ions determine redox-dependent anti-apoptotic effect of cerium oxide nanoparticles, ACS Nano 5 (6) (2011) 4537–4549.
[40] E.G. Heckert, A.S. Karakoti, S. Seal, W.T. Self, The role of cerium redox state in the SOD mimetic activity of nanoceria, Biomaterials 29 (18) (2008) 2705–2709.
[41] A. Migani, G.N. Vayssilov, S.T. Bromley, F. Illas, K.M. Neyman, Greatly facilitated oxygen vacancy formation in ceria nanocrystallites, Chem. Commun. 46 (32) (2010) 5936–5938.
[42] L. Xu, J. Liu, J. Xi, Q. Li, B. Chang, X. Duan, G. Wang, S. Wang, Z. Wang, L. Wang, Synergized multimodal therapy for safe and effective reversal of cancer multidrug resistance based on low-level photothermal and photodynamic effects, Small (2018), e1800785.
[43] M. Soh, D.W. Kang, H.G. Jeong, D. Kim, D.Y. Kim, W. Yang, C. Song, S. Baik, I. Y. Choi, S.K. Ki, H.J. Kwon, T. Kim, C.K. Kim, S.H. Lee, T. Hyeon, Ceria–zirconia nanoparticles as an enhanced multi-antioxidant for sepsis treatment, Angew. Chem., Int. Ed. 56 (38) (2017) 11399–11403.
[44] J. Li, S. Song, Y. Long, L. Wu, X. Wang, Y. Xing, R. Jin, X. Liu, H. Zhang, Investigating the hybrid-structure-effect of CeO_2-encapsulated Au nanostructures on the transfer coupling of nitrobenzene, Adv. Mater. 30 (7) (2018), 1704416.
[45] T. Liu, B. Xiao, F. Xiang, J. Tan, Z. Chen, X. Zhang, C. Wu, Z. Mao, G. Luo, X. Chen, J. Deng, Ultrasmall copper-based nanoparticles for reactive oxygen species scavenging and alleviation of inflammation related diseases, Nat. Commun. 11 (1) (2020) 2788.
[46] J. Liu, Q. Li, J. Zhang, L. Huang, C. Qi, L. Xu, X. Liu, G. Wang, L. Wang, Z. Wang, Safe and effective reversal of cancer multidrug resistance using sericin-coated mesoporous silica nanoparticles for lysosome-targeting delivery in mice, Small 13 (9) (2017), 1602567.
[47] T. Ohkusa, Production of experimental ulcerative colitis in hamsters by dextran sulfate sodium and changes in intestinal microflora, Nihon Shokakibyo Gakkai Zasshi 82 (5) (1985) 1327–1336.
[48] Y. Lee, K. Sugihara, M.G. Gillilland 3rd, S. Jon, N. Kamada, J.J. Moon, Hyaluronic acid-bilirubin nanomedicine for targeted modulation of dysregulated intestinal barrier, microbiome and immune responses in colitis, Nat. Mater. 19 (1) (2020) 118–126.
[49] W. Guo, M. Zhang, Z. Lou, M. Zhou, P. Wang, H. Wei, Engineering nanoceria for enhanced peroxidase mimics: a solid solution strategy, ChemCatChem 11 (2) (2019) 737–743.
[50] Y. Zhang, K. Zhou, Y. Zhai, F. Qin, L. Pan, X. Yao, Crystal plane effects of nano-CeO_2 on its antioxidant activity, RSC Adv. 4 (92) (2014) 50325–50330.
[51] H. Zhu, X. Ke, X. Yang, S. Sarina, H. Liu, Reduction of nitroaromatic compounds on supported gold nanoparticles by visible and ultraviolet light, Angew. Chem., Int. Ed. 49 (50) (2010) 9657–9661.
[52] W. Li, Y. Li, Z. Liu, N. Kerdsakundee, M. Zhang, F. Zhang, X. Liu, T. Bauleth-Ramos, W. Lian, E. Makila, M. Kemell, Y. Ding, B. Sarmento, R. Wiwattanapatapee, J. Salonen, H. Zhang, J.T. Hirvonen, D. Liu, X. Deng, H.A. Santos, Hierarchical structured and programmed vehicles deliver drugs locally to inflamed sites of intestine, Biomaterials 185 (2018) 322–332.
[53] B. Tirosh, N. Khatib, Y. Barenholz, A. Nissan, A. Rubinstein, Transferrin as a luminal target for negatively charged liposomes in the inflamed colonic mucosa, Mol. Pharm. 6 (4) (2009) 1083–1091.
[54] G. Canny, O. Levy, G.T. Furuta, S. Narravula-Alipati, R.B. Sisson, C.N. Serhan, S. P. Colgan, Lipid mediator-induced expression of bactericidal/permeability-

increasing protein (BPI) in human mucosal epithelia, Proc. Natl. Acad. Sci. U. S. A. 99 (6) (2002) 3902–3907.
[55] C.G.B. Peterson, E. Eklund, Y. Taha, Y. Raab, M. Carlson, A new method for the quantification of neutrophil and eosinophil cationic proteins in feces: establishment of normal levels and clinical application in patients with inflammatory bowel disease, Am. J. Gastroenterol. 97 (7) (2002) 1755–1762.
[56] Y. Lee, N. Kamada, J.J. Moon, Oral nanomedicine for modulating immunity, intestinal barrier functions, and gut microbiome, Adv. Drug Deliv. Rev. 179 (2021), 114021.
[57] G.F. Hankard, J.P. Cezard, Y. Aigrain, J. Navarro, M. Peuchmaur, CD44 variant expression in inflammatory colonic mucosa is not disease specific but associated with increased crypt cell proliferation, Histopathology 32 (4) (1998) 317–321.
[58] Y. Wang, X. Wang, Y. Lv, Y. Guo, M. He, M. Lan, Y. Zhao, F. Gao, A ROS-responsive fluorescent probe detecting experimental colitis by functional polymeric nanoparticles, Int. J. Pharm. 609 (2021), 121125.
[59] N.G. Kotla, I.L.M. Isa, S. Rasala, S. Demir, R. Singh, B.V. Baby, S.K. Swamy, P. Dockery, V.R. Jala, Y. Rochev, A. Pandit, Modulation of gut barrier functions in ulcerative colitis by hyaluronic acid system, Adv. Sci. 9 (4) (2022), e2103189.
[60] H.A. Bakshi, V. Mishra, S. Satija, M. Mehta, F.L. Hakkim, P. Kesharwani, K. Dua, D. K. Chellappan, N.B. Charbe, G. Shrivastava, S. Rajeshkumar, A.A. Aljabali, B. Al-Trad, K. Pabreja, M.M. Tambuwala, Dynamics of prolyl hydroxylases levels during disease progression in experimental colitis, Inflammation 42 (6) (2019) 2032–2036.
[61] H. Schroder, D.E. Campbell, Absorption, metabolism, and excretion of salicylazosulfapyridine in man, Clin. Pharmacol. Ther. 13 (4) (1972) 539–551.
[62] T. Sousa, V. Yadav, V. Zann, A. Borde, B. Abrahamsson, A.W.J. Basit, On the colonic bacterial metabolism of azo-bonded prodrugsof 5-aminosalicylic acid, J. Pharm. Sci. 103 (10) (2014) 3171–3175.
[63] B. Chami, N.J.J. Martin, J.M. Dennis, P.K. Witting, Myeloperoxidase in the inflamed colon: a novel target for treating inflammatory bowel disease, Arch. Biochem. Biophys. 645 (2018) 61–71.
[64] S.J. McKenzie, M.S. Baker, G.D. Buffinton, W.F. Doe, Evidence of oxidant-induced injury to epithelial cells during inflammatory bowel disease, J. Clin. Invest. 98 (1) (1996) 136–141.
[65] T. ten Hove, B. van den Blink, I. Pronk, P. Drillenburg, M.P. Peppelenbosch, S. J. van Deventer, Dichotomal role of inhibition of p38 MAPK with SB 203580 in experimental colitis, Gut 50 (4) (2002) 507–512.